Laboratory Studies of Evaporation and Energy Transfer Through a Wavy Air-Water Interface

P. A. MANGARELLA,[1] A. J. CHAMBERS,[2] R. L. STREET AND E. Y. HSU

Stanford University, Stanford, Calif.

(Manuscript received 13 March 1972, in revised form 21 September 1972)

ABSTRACT

Interfacial evaporation and energy flux are presented for a series of experiments in a laboratory wind wave flume (neutral stratification) with varying free stream velocity and with and without mechanically generated waves. Integral conservation or budget techniques are the means of flux determination. Fluxes normalized to a 6-cm height are independent of fetch, increase with wind speed, and decrease if mechanically generated waves are introduced. Excellent correspondence between normalized energy and mass transfer exists except for the case involving spray which causes a reduction in the thermal field.

1. Introduction

The energy and mass[3] transfer through the ocean-air interface subject to a turbulent wind has been studied thoroughly with some success, especially with the advent of improved instrumentation (cf. *Radio Science*, 1969). Nonetheless, some basic questions still exist as to mechanisms which may have an effect on fluxes but which cannot be isolated without great difficulty in the field environment. The effects of spray and swell on energy and mass flux are two such examples.

The desirability of controlling and adjusting the variables governing interfacial phenomena would appear to suggest a laboratory experiment. Accordingly, by measurement of a series of vertical profiles of humidity, temperature and velocity along a laboratory test section, energy and mass flux through the air water interface have been computed (Mangarella *et al.*, 1971).

2. Experimental apparatus and techniques

The laboratory facility utilized in this study was the Stanford University Hydraulics Laboratory wind, water-wave flume shown in Fig. 1 and discussed by Hsu (1965). The interior dimensions of the channel are approximately 35 m long, 1.93 m high and 0.91 m wide. The channel was half filled with water; the upper half of the channel was then the air flow section having an aspect ratio of about 1. Air was drawn through the test section by a centrifugal fan at the exit end of the channel. In addition to the wind waves created by the air flow over the water, mechanically generated waves can be produced by a vertical plate actuated by an electronically controlled hydraulic cylinder. Three evenly spaced 0.95-cm diameter chromolax electric heating cables near the floor of the channel heated the water. The air inlet configuration required an inclined plate with a 3-cm gap between the end of the plate and the water surface to allow for passage of the mechanically generated waves into the test section. The smooth aluminum plate was approximately 1.3 m long. To allow for a region of flow reattachment after the gap the initial station suitable for data taking was selected 3.2 m downstream.

An experimental run consisted of measuring the mean vertical profiles of temperature, horizontal velocity and humidity above the mean water level at eight locations along the channel (stations 3–10, Fig. 1). A completely automated traversing mechanism was built for this purpose. Auxiliary measurements included wave height, mean water level, and temperatures below the air-water boundary.

Standard pitot-static tubes were used for the velocity measurement, thermistor beads for temperature, and humidity-sensitive variable resistors (Hygrodynamics, Inc.) for relative humidity. Wave height was measured with a capacitance gage. The temperature of that fluid very close to the interface was determined with an infrared radiometer (Barnes Engineering Model PRT-5) provided by the Remote Sensing Laboratory, Department of Geophysics, Stanford University.

The primary variables investigated were wind speed, fetch and wave configuration, i.e., wind waves versus a combination of wind and mechanically generated waves (see Table 1). Boundary layer growth along the test section accelerated the core velocity as much as 10% from stations 3 to 10 and therefore wind velocities

[1] Present affiliation: University of Massachusetts, Amherst, Mass.

[2] Present affiliation: University of Newcastle, New South Wales, Australia.

[3] Unless otherwise noted mass refers to water vapor.

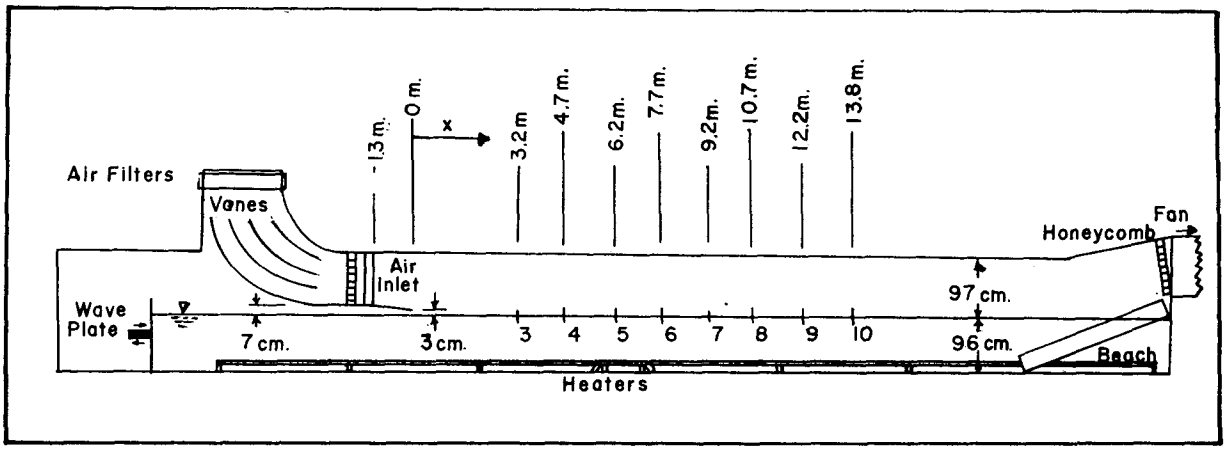

FIG. 1. Wind, water-wave flume.

stated are referenced to Station 6, the approximate mid-point of the test section. Temporal variations of air and surface water temperatures existed because of atmospheric changes in the inlet temperature, and for Test 4 the inability of the heaters to compensate for the energy losses of the water. The water-air temperature difference for Test 4 varied from 14 to 10.6C through the period of the experiment (~3 hr). A steady-state hypothesis is entirely valid for such long-term variations.

3. Integral flux measuring principle

The integral conservation method was used to determine the flux through the interface on the basis of an energy or mass budget applied to a control volume above the mean water level (Appendix B). The technique is based on the principal of measuring all flux components except for the unknown interfacial flux, be it evaporation or energy. For steady, two-dimensional flow and constant free stream and interface specific humidity, the integral mass transfer equation (B6) is

$$\mathrm{St}_m = \frac{d\Omega}{dx} + \frac{\Omega}{u_\infty}\frac{du_\infty}{dx} - \frac{\rho_0 w_0}{\rho_\infty u_\infty}. \tag{1}$$

TABLE 1. Range of variables.

Test	U_∞ (m sec)	Station 6 $T_0{}^*-T_\infty$ (°C)	T_0 (°C)	Mechanically generated wave Height (initial) (cm)	Frequency (Hz)
1	3.6	15.3	37.7	none	
2	6.6	14.9	33.3	none	
3	11.1	11.5	31.8	none	
4	14.5	12.2	27.6	none	
5	3.4	14.1	37.6	3.2	1.2
6	6.4	17.4	29.7	1.9	1.2
7	6.6	14.2	33.0	3.2	1.2
8	10.6	15.0	31.6	3.2	1.2

* Determined from radiometer.

The mass transfer Stanton number

$$\mathrm{St}_m = E/[\rho_\infty u_\infty (q_0 - q_\infty)]$$

is the normalized evaporation rate E (see Appendix A for nomenclature). The term $d\Omega/dx$ where Ω is the integral concentration thickness represents the net increase in horizontal convected mass across the control volume, and $(\Omega/u_\infty)(du_\infty/dx)$ is the pressure gradient term. The last term, $\rho_0 w_0/(\rho_\infty w_\infty)$, represents normalized convective mass flux through the interface caused by and related to evaporation by (B9), i.e.,

$$\rho_0 w_0/(\rho_\infty u_\infty) = B\ \mathrm{St}_m, \tag{2}$$

where B is called the mass transfer driving force, i.e., $B=(q_0-q_\infty)/(1-q_0)$. With this expression for $\rho_0 w_0/(\rho_\infty u_\infty)$, Eq. (1) becomes

$$\mathrm{St}_m = [(d\Omega/dx + (\Omega/u_\infty)(du_\infty/dx)]/(1+B). \tag{3}$$

Eq. (3) in terms of Reynolds numbers $\mathrm{Re}_\Omega = u_\infty \Omega/\nu$ and $\mathrm{Re}_x = u_\infty x/\nu$ is

$$\mathrm{St}_m = (1+K\ \mathrm{Re}_x)(d\ \mathrm{Re}_\Omega/d\ \mathrm{Re}_x)/(1+B), \tag{4}$$

where K is a pressure gradient term, $K=(\nu/u_\infty{}^2)(du_\infty/dx)$. The mass Stanton number was determined by experimentally evaluating the right-hand side of Eq. (4). The concentration thickness is

$$\Omega = \int_0^{\bar{z}} (\rho u/\rho_\infty u_\infty)[1-(q-q_0)/(q_\infty - q_0)]dz, \tag{5}$$

and can be evaluated from the mean vertical profiles of velocity u, density ρ, and specific humidity q.

An equation similar to Eq. (4) can be derived for energy transfer where the appropriate conserved property is the enthalpy i of the binary (air and water vapor) mixture. Energy transfer in a binary mixture is associated with mass as well as thermal diffusion and the resulting integral energy conservation equation is more complex than the corresponding mass conservation equation. Fortunately, if the turbulent and laminar

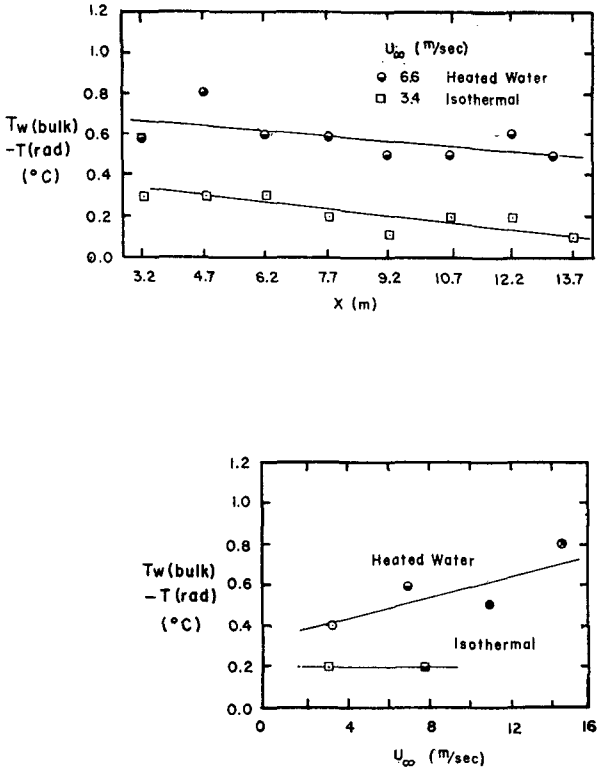

FIG. 2. Bulk water-interface temperature difference vs fetch, a., and wind speed, b.

Lewis numbers, Le_t and Le, are close to unity, the energy integral equation can be simplified to a form similar to Eq. (4). The Lewis numbers are the ratio of the mass and thermal diffusion coefficients. For the air and low water vapor concentration mixture encountered here Le is approximately 1.16. Hogstrom (1967) found that the turbulent Lewis number was approximately unity for neutrally stable conditions over the ocean.

Thus, the assumptions of unity for Lewis numbers appear to be valid for these experimental conditions. With these assumptions and those used in deriving Eq. (4), the Reynolds number form of the energy integral equation is

$$\mathrm{St}=(1+K\ \mathrm{Re}_x)(d\ \mathrm{Re}_\theta/d\ \mathrm{Re}_x)/(1+B), \qquad (6)$$

where $\mathrm{St}=I/[\rho_\infty u_\infty(i_0-i_\infty)]$, I is the interfacial energy transfer, the enthalpy thickness is

$$\theta=\int_0^{\bar{z}}(\rho u/\rho_\infty u_\infty)[1-(i-i_0)/(i_\infty-i_0)]dz, \qquad (7)$$

and i is the mixture enthalpy. The enthalpy datum were chosen as follows: air, $i_a=C_{p_a}(T-T_0)$; water vapor, $i_{wv}=L_{T_0}+C_{p_{wv}}(T-T_0)$. The specific heats for air and saturated water vapor are C_{p_a} and $C_{p_{wv}}$, respectively, and L_{T_0} is the latent heat of vaporization for water at the interface temperature T_0. The mixture enthalpy therefore was

$$i=(1-q)[C_{p_a}(T-T_0)]+q[L_{T_0}+C_{p_{wv}}(T-T_0)], \qquad (8)$$

where $1-q$ is the mass concentration of air and q the mass concentration of water vapor or specific humidity. The enthalpy datum were chosen such that the water vapor enthalpy at the interface was $i_{wv,0}=L_{T_0}$ to be consistent with the meteorological practice of determining the energy associated with evaporation as $L_{T_0}E$. The enthalpy thickness was evaluated from the experimental data using Eqs. (7) and (8). With the above enthalpy datum choices, I represents total energy transfer including that energy associated with the liquid to water vapor phase change at the interface.

As previously mentioned Eqs. (4) and (6) rely on the assumption that T_0 and q_0 are constant with fetch. The validity of this assumption is brought out in Fig. 2a which shows that the interfacial temperature gradient is of the order of 0.02C m^{-1} for a wind speed of 6.6 m sec^{-1}. Similar results were found for other wind speeds. The so-called skin temperature effect or depression of the interfacial temperature due to energy transfer is also shown in Fig. 2b for a range of wind speeds. The skin temperature depression is seen to increase with wind speed (and evaporation rate) as would be expected. Isothermal results (water unheated) are shown in these figures for comparison.

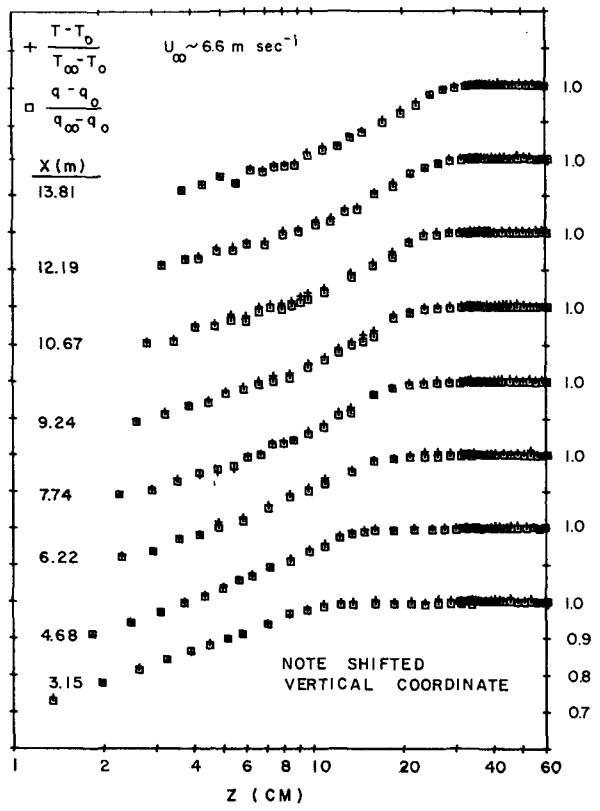

FIG. 3. Normalized water vapor and temperature profiles above the mean water level: heated water, wind waves only.

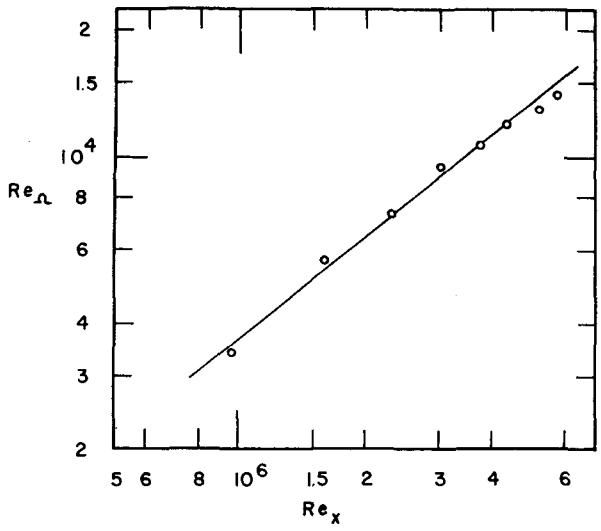

FIG. 4. Concentration thickness Reynolds number vs Reynolds number based on distance from inlet.

4. Experimental results

a. *Profile, integral parameter, and Stanton number relations*

Fig. 3 shows a typical set of normalized temperature and water vapor concentration data taken over the air-water interface. The observed similarity between the normalized thermal[4] and water vapor concentration profiles can be predicted on the basis of the similarity between the energy and water vapor conservation differential equations and boundary conditions under the Lewis numbers unity assumptions. Thus, the similar profile results appear to justify these assumptions which were used in developing Eq. (6) and further substantiate the common hypothesis that the processes governing energy and water vapor transfer are similar under neutral stratification.

A typical concentration Reynolds number distribution is shown in Fig. 4. The origin for x used in evaluating Re_x was determined by extrapolating the appropriate integral parameter variation back to where its value was zero. These data were represented with a least-squares fit curve of the form

$$\mathrm{Re}_\Omega = a\,\mathrm{Re}_x^b, \tag{9}$$

as shown in Fig. 4. Enthalpy thickness data were fit in a similar fashion. It is important to appreciate that the enthalpy datum choices do not influence the normalized enthalpy $(i-i_0)/(i_\infty-i_0)$ and therefore the enthalpy thickness θ if the Lewis numbers unity assumptions are valid. This is not true in general and specifically was not true in these experiments for Test 4 which involved spray.

[4] Numerical results showed that enthalpy profiles computed from similar concentration and thermal profiles were also similar.

Stanton numbers were computed using Eqs. (4) and (6) with the concentration and enthalpy thicknesses as given by Eqs. (5) and (7). Fig. 5 shows Stanton number vs Reynolds number based on concentration or enthalpy thickness for the wind wave cases. The linear relation of Stanton number to Reynolds number is dictated by the fitting technique [Eq. (9)]. The low wind speed case ($u_\infty \approx 3.6$ m sec^{-1}) hardly disturbed the water surface and the close Stanton number agreement with the flat porous plate results of Whitten (1967) is not surprising. The intermediate wind speed cases ($u_\infty \approx 6.6$, 11.1 m sec^{-1}) substantially roughened the interface causing about a 50% increase in Stanton number over the 3.6 m sec^{-1} case. The Stanton numbers for both intermediate wind speed cases form one continuous band of data pointing out perhaps the appropriateness of this Reynolds number scaling for certain wind speed regimes.

Fig. 6 shows the flux data for cases involving mechanically as well as wind generated waves. The Stanton numbers generally lie between the previously discussed low and intermediate wind speed, wind wave cases. These data exhibit somewhat more scatter than the wind wave data as it was not possible to sample data near the mean water level because of the mechanically generated wave presence.

b. *The effects of spray*

Lai and Plate (1969) and Okuda and Hayami (1959) have observed the creation of spray at wind speeds >11 m sec^{-1}. In the tests reported here significant amounts of spray were not observed in those runs having a wind speed of 11 m sec^{-1}. This is not in conflict with the above mentioned researchers as 11 m sec^{-1} is a threshold value only.

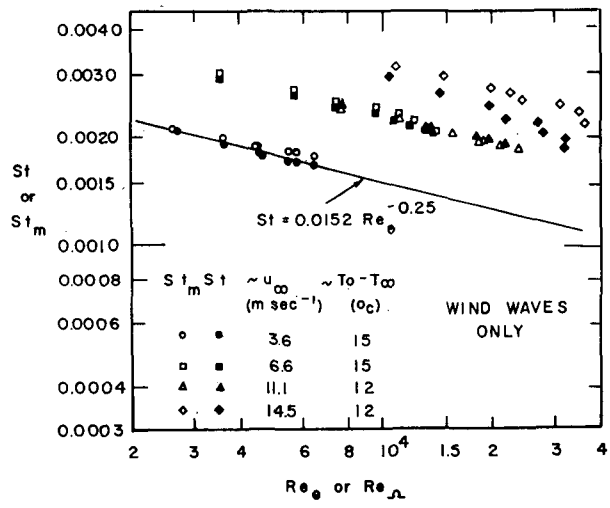

FIG. 5. Energy and mass transfer Stanton number vs enthalpy and concentration Reynolds number, respectively. Solid line represents flat, porous plate heat transfer results of Whitten (1967).

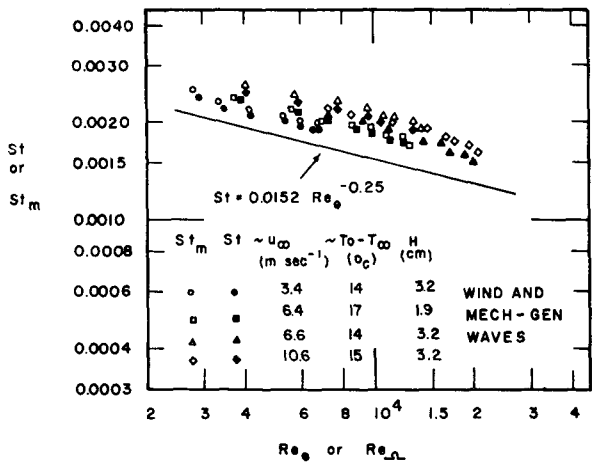

FIG. 6. Energy and mass transfer Stanton number vs enthalpy and concentration Reynolds number, respectively. Solid line represents flat, porous plate heat transfer results of Whitten (1967).

In Test 4 (wind speed 14.5 m sec^{-1}) spray was observed, especially at stations 7–10. Strobe light flashes directed across the channel at these stations indicated large numbers of spray droplets throughout the boundary layer. Humidity sensors were protected from droplets by a membrane covering pervious to air and water vapor only. The thermistors had a diameter (2.5 mm) small enough to avoid droplet effects for the most part. When thermistor-droplet interaction was noted the data record was omitted from analysis.

This was the only test in which a significant departure between the normalized thermal and water vapor concentrations was observed. Fig. 7 shows the dissimilarity in profiles arising from the spray evaporation which converts energy from the thermal to the water vapor concentration field. The temperature drop in the presence of spray may be estimated as to order of magnitude from Fig. 7 if we assume that the normalized temperature distribution without spray lies approximately in between the observed profiles shown in Fig. 7. Then the difference in normalized temperature for station 10 (elevation 10 cm) with and without spray is approximately 0.025. For the interfacial free-stream temperature difference of 12.2C corresponding to this case, the temperature drop due to spray is of the order of 0.3C. This estimate is probably low as the thermal field is more sensitive to spray evaporation (through latent heat release) than the concentration field.

The appropriate energy and mass conservation equations with spray must include the transport associated with spray particles. One must differentiate between the mass concentrations of air, water vapor and liquid water. Additional terms in the integral equations arise which cannot be evaluated without droplet spray concentration profiles and spray generation rates at the interface. Toba (1961), Blanchard (1963), and Monahan (1968) and others have contributed to the resolution of these questions. However, the synthesis of the various elements of spray flow in a boundary layer with the linked energy and mass conservation equations has yet to be accomplished. For the present we have chosen to use Eqs. (4) and (6) to represent the equivalent Stanton numbers which include the effect of spray on mass and energy transfer. Fig. 5 shows the equivalent and higher Stanton numbers for the spray case.

c. Diffusion layer properties

Diffusion layer thicknesses δ were generated from the experimental data using an evaporation prediction equation of Sverdrup [Eq. (33), 1951] in the form:

$$\frac{[C_f(6)]^{\frac{1}{2}}}{\mathrm{St}_m(6)} = \mathrm{Sc}\xi^* + \frac{1}{[C_f(6)]^{\frac{1}{2}}} + \frac{1}{k}\ln[z_0^*/(z_0^*+\delta^*)], \quad (10a)$$

for rough flow, $z_0^* \geq 2$, and

$$\frac{[C_f(6)]^{\frac{1}{2}}}{\mathrm{St}_m(6)} = \mathrm{Sc}\delta^* + \frac{1}{[C_f(6)]^{\frac{1}{2}}} + \frac{1}{k}\ln k\,\mathrm{Sc} - 5.5 \quad (10b)$$

for smooth flow, $z_0^* < 2$.

The Stanton number $\mathrm{St}_m(6)$ and drag coefficient $C_f(6)$ are referenced to a height of 6 cm and $z_0^* = u_* z_0/\nu$

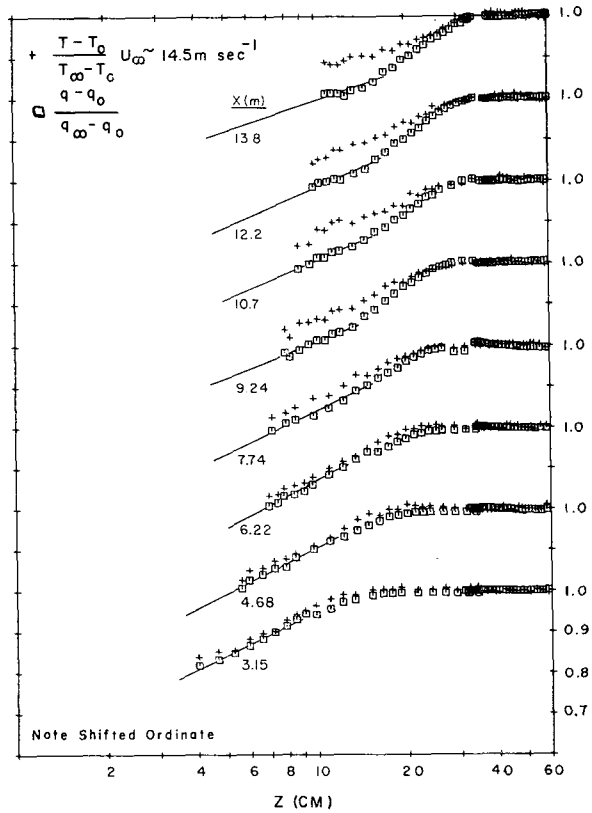

FIG. 7. Normalized water vapor and temperature profiles above the mean water level: heated water, wind waves with spray.

TABLE 2. Fetch-averaged data.

Data set	6 cm height					10 m height (extrapolated)	
	$St_m(6)$	$C_f(6)^{\frac{1}{2}}$	u_* (cm sec^{-1})	z_0 (cm)	u_*z_0/ν	$u(10)$ (m sec^{-1})	$St_m(10)$
1	0.0026	0.045	14	0.001	1.0	4.9	0.0007
2	0.0037	0.071	37	0.023	5.6	10.0	0.0014
3	0.0032	0.074	63	0.030	12.6	16.9	0.0012
4	0.0047	0.129	130	0.271	234.0	27.4	0.0033
5	0.0030	0.046	14	0.001	1.0	4.7	0.0008
6	0.0029	0.084	44	0.052	15.0	6.2	0.0013
7	0.0033	0.055	30	0.002	0.4	9.0	0.0009
8	0.0030	0.099	77	0.102	52.0	18.2	0.0015

and $\delta^*=u_*\delta/\nu$. The shear velocity was determined from the profile technique. Eqs. (10) were applied for each experiment to the fetch-averaged Stanton number and drag coefficient (Table 2).

Fig. 8 shows the diffusion layer thicknesses generated using Eq. (10) vs wind speed at 10 m [extrapolated logarithmically using u(6 cm) and z_0] compared with the findings of Schooley (1971) in a smaller laboratory channel. The diffusion layer thicknesses for wind wave tests (indicated by the dashed line) are much higher than Schooley's data for high wind speeds. Separation phenomena (which are reflected in the diffusion layer thickness concept) more prevalent in the large fetch situations probably account for these differences. Schooley's data support the classical diffusion layer hypothesis, namely $\delta u_*/\nu=$constant, which may be inconsistent with the mobile interface (particularly at large fetches) except for low wind speeds as indicated in Fig. 8.

The diffusion thicknesses for a combination of generated and wind waves are somewhat ambiguous, related no doubt to the uncertainty in determining u_* and z_0 from profile data necessarily taken well above the mean water level. Nonetheless, the shear velocity over mechanically generated and wind waves is greater than over wind waves alone (except for Test 7) consistent with the results of Shemdin and Lai (1971). Except for the low-wind-speed case, the diffusion thicknesses for generated waves are larger than the corresponding wind wave cases. This may be due to a sheltering effect on the high-frequency wave structure (Bole and Hsu, 1967) which incidentally is not reflected in the profile determinations of z_0. Such a sheltering effect would play a minor role in the low speed case.

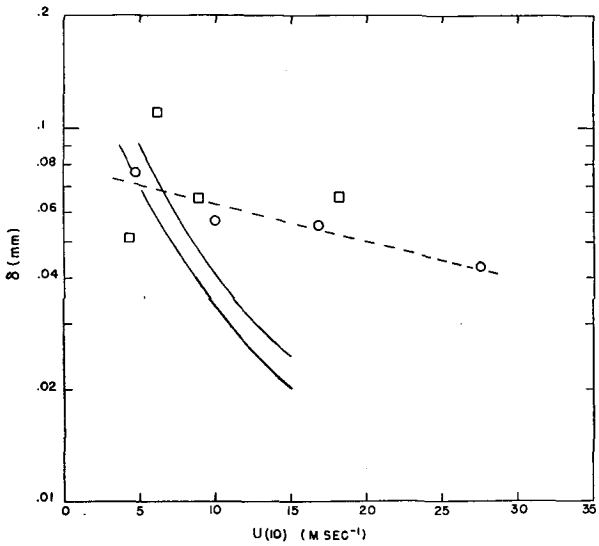

FIG. 8. Diffusion layer thickness vs wind speed at 10 m: ○, wind waves; □, wind and mechanically generated waves. Solid line is from Schooley (1971).

Diffusion thicknesses associated with energy transfer would be approximately identical to those computed for mass transfer and therefore have not been shown.

Stanton numbers referenced to a 10 m height have been extrapolated logarithmically using St_m(6 cm) and z_0 and are tabulated in Table 2 and plotted in Fig. 9 versus roughness Reynolds number u_*z_0/ν. The average Stanton number of 0.00123 found by Pond *et al.* (1971) using eddy correlation techniques in the field agrees with these data in the central flow regime.

5. Conclusions

1. The integral conservation technique is a viable method of energy and mass flux determination in a laboratory channel.

2. The normalized energy and mass transfer coefficients (presented in Stanton number form) may be considered equal for the neutrally stable conditions studied here except for the case involving spray.

3. The Stanton numbers referenced to free-stream conditions (i) decreased with fetch for a given wind speed and (ii) increased with wind speed at a given fetch. However the Stanton numbers referenced to a height of 6 cm (well within the boundary layer) were fetch-independent for a given wind speed.

4. Spray droplets evaporating in the boundary layer cause a reduction in the thermal profiles on the order of 0.3C and a corresponding increase in water vapor concentration. It was not possible, however, to identify that portion of the increased evaporation due to spray alone.

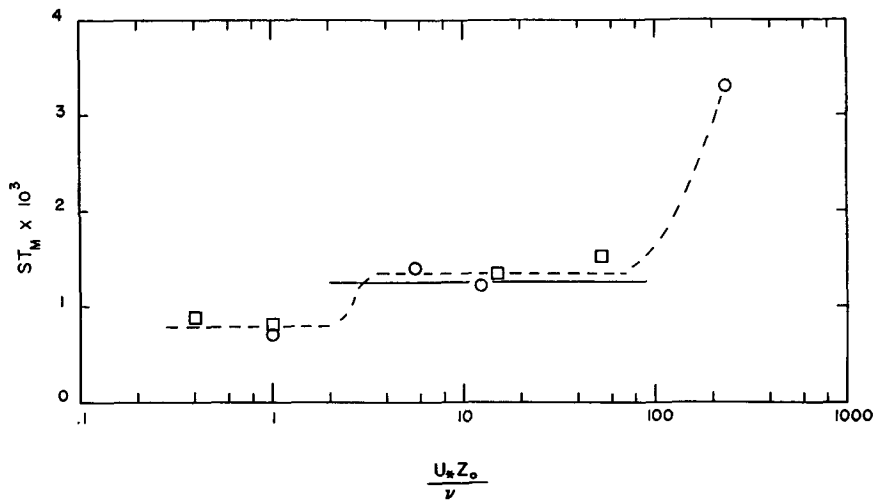

FIG. 9. Evaporation Stanton number at 10 m (extrapolated) vs roughness Reynolds number: ○, wind waves; □, wind and mechanically generated waves. Solid line is from Pond *et al.* (1971).

5. Diffusion layer thicknesses were found to be approximately constant rather than decreasing according to the common hypothesis $u_*\delta/\nu = \text{constant}$.

6. The effect of mechanically generated waves would appear to reduce the evaporation and energy transfer from that which would occur with wind waves alone; however, additional research is needed to clarify these effects.

7. Average Stanton numbers extrapolated to a 10 m height correlate with roughness Reynolds indicating three regimes of flow: smooth, fully rough, and fully rough with spray.

Acknowledgments. The authors wish to express their thanks to Prof. R. J. Moffat, Dept. of Mechanical Engineering, Stanford University, for his very helpful suggestions on enthalpy datum considerations and mass and energy transport with spray. This work was supported by the Atmospheric Sciences Section, National Science Foundation, under Grant GA-1471.

APPENDIX A

Nomenclature

B	mass transfer driving force, $(q_\infty - q_0)/(q_0 - 1)$
C_f	skin friction, u_*^2/u^2
C_p	specific heat
E	evaporation rate
I	total energy transfer rate
i	enthalpy: see Eq. (8)
K	pressure gradient term, $(\nu/u_\infty^2)(du_\infty/dx)$
Le	Lewis number, ratio of mass to thermal diffusion coefficients
L	latent heat
q	specific humidity
$\bar{q}$	normalized specific humidity, $(q_0 - q)/(q_0 - q_\infty)$
Re_x	Reynolds number, $u_\infty x/\nu$
Re_Ω	Reynolds number, $u_\infty \Omega/\nu$
Re_θ	Reynolds number, $u_\infty \theta/\nu$
St	Stanton number or normalized energy transfer rate, $I/\rho u(i_0 - i)$
St_m	Stanton number or normalized evaporation rate, $E/\rho u(q_0 - q)$
Pr	Prandtl number, ratio of momentum to thermal diffusion coefficient
Sc	Schmidt number, ratio of momentum to water vapor diffusion coefficient
T	temperature
u	velocity in streamwise direction
u_*	shear velocity
w	vertical velocity component
x, y, z	coordinate axes
$\bar{z}$	some height greater than boundary layer thickness
z_0	roughness height
δ	diffusion layer thickness
θ	enthalpy thickness: see Eq. (7)
ν	kinematic viscosity of air-water vapor mixture
ρ	air-water vapor mixture density
Ω	water vapor concentration thickness: see Eq. (5)

subscripts

a	air
t	turbulent
wv	water vapor
0	evaluated at the interface
∞	evaluated in free stream

superscripts

*	Reynolds number formed with shear velocity

APPENDIX B

Water Vapor Integral Equation[5]

Consider the control volume shown in Fig. 10a assumed to begin immediately above the mean water

[5] Development follows Kays (1966).

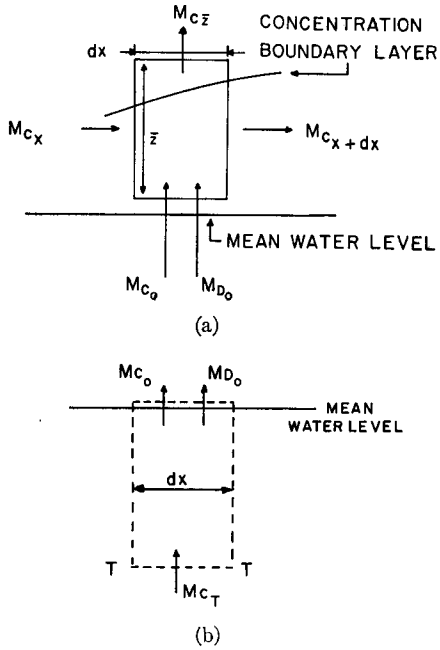

FIG. 10. Boundary layer control volume (a) and T state control volume (b) for water vapor conservation integral equation.

level and extend a distance $\bar{z}$ above the mean water level. Here $\bar{z}$ is some distance greater than the concentration boundary layer thickness. The appropriate contributing terms for water-vapor conservation for two dimensional, steady flow are:

1) Convected flux of water vapor along with the mean stream flow

$$Mc_x = dy \int_0^{\bar{z}} \rho u q dz$$

$$Mc_{x+dx} = dy\left[\int_0^{\bar{z}} \rho u q dz + \frac{d}{dx}\left(\int_0^{\bar{z}} \rho u q dz\right)dx\right]$$

2) Convected flux of water vapor through the interface

$$Mc_0 = \rho_0 w_0 q_0 dx dy$$

3) Convected flux of water vapor through the $\bar{z}$ surface

$$Mc_{\bar{z}} = \rho_{\bar{z}} w_{\bar{z}} q_\infty dx dy$$

4) Diffusive flux of water vapor through the interface

$$Md_0 = E dx dy = -\rho(D+D_t)\left.\frac{\partial q}{\partial z}\right|_{z=0} dx dy$$

Applying conservation of water vapor to the control volume, we have

(Entering control volume)

$$dy \int_0^{\bar{z}} \rho u q dz + \rho_0 w_0 q_0 dx dy + E dx dy$$

(Leaving control volume)

$$= dy\left[\int_0^{\bar{z}} \rho u q dz + \frac{d}{dx}\left(\int_0^{\bar{z}} \rho u q dz\right)dx\right] + \rho_{\bar{z}} w_{\bar{z}} q_\infty dx dy. \quad \text{(B1)}$$

Dividing Eq. (B1) by $dxdy$ and simplifying, we have

$$\rho_0 w_0 q_0 + E = \frac{d}{dx}\int_0^{\bar{z}} \rho u q dz + \rho_{\bar{z}} w_{\bar{z}} q_\infty. \quad \text{(B2)}$$

If we apply conservation of total mass to the control volume, we obtain

$$\rho_{\bar{z}} w_{\bar{z}} = \rho_0 w_0 - \frac{d}{dx}\int_0^{\bar{z}} \rho u dz. \quad \text{(B3)}$$

Using this expression for $\rho_{\bar{z}} w_{\bar{z}}$ in Eq. (B2) yields

$$\rho_0 w_0 (q_0 - q_\infty) + E = \frac{d}{dx}\int_0^{\bar{z}} \rho u (q - q_\infty) dz. \quad \text{(B4)}$$

If we assume that $(q_0 - q_\infty)$ is not a function of x and divide by $\rho_\infty u_\infty (q_0 - q_\infty)$, we have

$$\frac{\rho_0}{\rho_\infty}\frac{w_0}{u_\infty} + \frac{E}{\rho_\infty u_\infty (q_0 - q_\infty)} = \frac{1}{u_\infty}\frac{d}{dx}\int_0^{\bar{z}} \frac{\rho u (q - q_\infty)}{\rho_\infty (q_0 - q_\infty)} dz. \quad \text{(B5)}$$

In terms of mass Stanton number,

$$\mathrm{St}_m = E/[\rho_\infty u_\infty (q_0 - q_\infty)],$$

and concentration ratio, $\bar{q} = (q - q_0)/(q - q_0)$, this equation becomes after rearrangement

$$\mathrm{St}_m = \frac{\Omega}{u_\infty}\frac{du_\infty}{dx} + \frac{d\Omega}{dx} - \frac{\rho_0 w_0}{\rho_\infty u_\infty}, \quad \text{(B6)}$$

where Ω is the integral parameter concentration thickness, i.e.,

$$\Omega = \int_0^{\bar{z}} \frac{\rho}{\rho_\infty}\frac{u}{u_\infty}(1 - \bar{q}) dz.$$

Now consider the control volume shown in Fig. 10b extending from just above the mean water level to well below the mean water level. Conservation of water (liquid and vapor phases) applied to this control volume requires that

$$Mc_0 + Md_0 = Mc_T, \quad \text{(B7)}$$

where T used as a subscript denotes the T surface of

the control volume. This surface is assumed to be far enough below the mean water level that no thermal or concentration gradients exist; therefore, convective transport is the only transport mode possible through the T surface. The symbol Mc_T denotes the convective water vapor through the T surface. Providing the appropriate expressions for each of the terms in Eq. (B7) we have

$$\rho_0 w_0 q_0 dxdy + Edxdy = \rho_0 w_0 q_T dxdy, \tag{B8}$$

where the water vapor concentration at the T state must be one, i.e., $q_T=1$, because there is no other specie at the T surface except liquid water. Note that the total flux of water vapor through the air-water interface as expressed by the terms on the left-hand side of Eq. (B8) consists of two parts, convective and diffusive flux. Thus, the diffusive flux E (or the normalized flux as represented by St_m) is not the total flux of water vapor through the interface. Dividing by $\rho_\infty u_\infty (q_0-q_\infty)$, Eq. (B8) becomes

$$\frac{\rho_0}{\rho_\infty}\frac{w_0}{u_\infty} = \frac{q_\infty - q_0}{q_0 - q_T}\frac{E}{\rho_\infty u_\infty (q_0-q_\infty)},$$

or

$$\frac{\rho_0 w_0}{\rho_\infty u_\infty} = B\ \mathrm{St}_m, \tag{B9}$$

where $B=(q_\infty-q_0)/(q_0-q_T)$ is called the mass transfer driving force.[6] Putting this expression for $\rho_0 w_0/\rho_\infty u_\infty$ in Eq. (B6) yields

$$\mathrm{St}_m = \left[\frac{\Omega}{u_\infty}\frac{du_\infty}{dx} + \frac{d\Omega}{dx}\right] \Big/ (1+B). \tag{B10}$$

This is the water vapor conservation integral equation for steady, two-dimensional flow and q_0 and q_∞ constant with x.

[6] Spalding (1963) discusses the significance of B in a variety of mass transfer applications.

REFERENCES

Blanchard, D. C., 1963: Electrification of the atmosphere. *Progress in Oceanography*, Vol. 1, Pergamon Press, 71–202.

Bole, J. B., and E. Y. Hsu, 1967: Response of gravity water waves to wind excitation. Tech. Rept. No. 79, Dept. of Civil Engineering, Stanford University.

Hogstrom, U., 1967: Turbulent water vapor transfer at different stability conditions. *Phys. Fluids Suppl.*, S247–S254.

Hsu, E. Y., 1965: A wind water-wave research facility. Tech. Rept. No. 57, Dept. of Civil Engineering, Stanford University.

Kays, W. M., 1966: *Convective Heat and Mass Transfer*. New York, McGraw-Hill, 387 pp.

Lai, R. J., and E. J. Plate, 1969: Evaporation from small wind waves. Rept. No. CER68-69JRL35, Dept. of Civil Engineering, Colorado State University.

Mangarella, P. A., A. J. Chambers, R. L. Street and E. Y. Hsu, 1971: Energy and mass transfer through an air-water interface. Tech. Rept. No. 134, Dept. of Civil Engineering, Stanford University.

Monahan, E. C., 1968: Sea spray as a function of low elevation wind speed. *J. Geophys. Res.*, **73**, 1127–1137.

Okuda, S., and S. Hayami, 1959: Experiments on evaporation from wavy water. *Records Oceanog. Works, Japan*, **5**, 6–13.

Pond, S., G. T. Phelps, J. E. Paquin, G. McBean and R. W. Stewart, 1971: Measurement of the turbulent fluxes of momentum, moisture and sensible heat over the ocean. *J. Atmos. Sci.*, **28**, 901–917.

Radio Science, 1969: Proceedings of colloquium on spectra of meteorological variables, Stockholm. 9–19 June, Vol. 4, No. 12.

Schooley, A. H., 1971: Diffusion sublayer thickness over wind-disturbed water surfaces. *J. Phys. Oceanogr.*, **1**, 221–223.

Shemdin, O. H., and R. J. Lai, 1971: Laboratory investigations of air turbulence above simple water waves. *J. Geophys. Res.*, **76**, 7334–7350.

Spalding, D. B., 1963: *Convective Mass Transfer*. New York, McGraw-Hill, 448 pp.

Sverdrup, H. V., 1951: Evaporation from the oceans. *Compendium of Meteorology*, Boston, Amer. Meteor. Soc., 1071–1081.

Toba, Y., 1961: Drop production by bursting of air bubbles on the sea surface (III), Study by use of a wind flume. *Mem. Coll. Sci., Univ. Kyoto*, **A29**, 313–344.

Whitten, D. G., 1967: The turbulent boundary layer on a porous plate: Experimental heat transfer with variable suction, blowing, and surface temperature. Ph.D. thesis, Thermosciences Div., Mech. Engineering Dept., Stanford University.